Post-Combustion CO2 Capture by Vacuum Swing Adsorption Using Zeolites – a Feasibility Study

G. D. Pirngruber, V. Carlier, D. Leinekugel-Le-Cocq

DOSSIER Edited by/Sous la direction de : **P.-L. Carrette**

PART 2
Post Combustion CO$_2$ Capture
Captage de CO$_2$ en postcombustion

ifp Energies nouvelles

Post-Combustion CO$_2$ Capture by Vacuum Swing Adsorption Using Zeolites – a Feasibility Study

G. D. Pirngruber*, V. Carlier and D. Leinekugel-le-Cocq

IFP Energies nouvelles, Rond-point de l'échangeur de Solaize, BP 3, 69360 Solaize - France
e-mail: gerhard.pirngruber@ifpen.fr - vincent.carlier27@gmail.com - damien.leinekugel@ifpen.fr

* Corresponding author

Résumé — **Captage du CO$_2$ en postcombustion par adsorption modulée en pression avec désorption sous vide sur zéolithes** — **étude de faisabilité** — Les résultats de simulation issus de la littérature suggèrent que les procédés d'adsorption modulée en pression avec désorption sous vide (*Vacuum Swing Absorption*, VSA) employant un physisorbant sont nettement moins efficaces d'un point de vue énergétique que le procédé de référence de captage de CO$_2$ par absorption aux amines. La plupart des études considèrent la zéolithe NaX comme adsorbant. La NaX présente une très forte affinité pour le CO$_2$, mais elle est difficile à régénérer et est très sensible à la présence d'eau dans les fumées. Jouer sur la polarité de l'adsorbant doit permettre de trouver un meilleur compromis entre capacité d'adsorption, caractère régénérable et sensibilité à l'eau. C'est pourquoi, dans cette contribution, nous avons testé une série de zéolithes afin d'évaluer leur performances comme physisorbants dans un procédé de captage de CO$_2$ par VSA. Les adsorbants sont testés par adsorption de fumées modèles séches et humides sur un lit d'adsorbant, en perçage et en conditions cycliques. Le matériau le plus intéressant, la zéolithe EMC-1, est choisi pour la simulation d'un cycle VSA complet, en comparaison avec la NaX. Les deux adsorbants atteignent les objectifs en termes de rendement (> 90 %) et de pureté du CO$_2$ (> 95 %), mais le très faible niveau de pression nécessaire à la régénération de l'adsorbant sera un handicap de poids pour l'utilisation de cette technologie à grande échelle.

Abstract — *Post-Combustion CO$_2$ Capture by Vacuum Swing Adsorption using Zeolites —* *a Feasibility Study* — *Simulation results in the literature suggest that Vacuum Swing Adsorption (VSA) processes using physisorbents might largely outperform the current state-of-the-art post-combustion CO$_2$ capture technologies based on amine solvents in terms of energy consumption. Most studies consider the zeolite NaX as adsorbent. NaX has a very strong affinity for CO$_2$ but is difficult to regenerate and very sensitive to the presence of water in the flue gas. By tuning the polarity of the adsorbent, it might be possible to find a better compromise between adsorption capacity, regenerability and sensitivity to H$_2$O. In the present contribution, we therefore screen the performance of a series of zeolites as physisorbents in a VSA process for CO$_2$ capture. The adsorbents are tested by breakthrough experiments of a dry and wet model flue gas, in once-through and cyclic operation. The most interesting material, zeolite EMC-1, is selected for numerical simulations of a full VSA cycle, in comparison with zeolite NaX. Both solids satisfy the performance targets in terms of recovery ($> 90\%$) and purity of CO$_2$ ($> 95\%$) but the very low pressure required for regeneration of the adsorbents will be a serious handicap for the deployment of this technology on a large scale.*

INTRODUCTION

There is now general consensus that the concentration of CO_2 in the atmosphere needs to be stabilized at a level of 450 ppm in order to limit the extent of global warming. In order to achieve this target, a series of measures will be necessary: increasing energy efficiency, shifting to energy sources that produce little or no CO_2 emissions (wind, solar, nuclear, biomass, etc.) and, last but not least, employing CCS technology (Carbon Capture and Storage) to large CO_2 emitters, in particular to coal firing power plants. Scenarios show that a ~ 20% contribution of CCS is needed in order to stabilize the CO_2 concentration at the desired level. There are different ways to deploy CCS: one distinguishes oxy-combustion, pre-combustion CO_2 capture and post-combustion CO_2 capture. We are here concerned with post-combustion CO_2 capture, which is the technology that can be most easily applied in existing coal/petroleum firing power plants, refineries, etc., by "simply" adding a CO_2 capture unit to the plant. Post-combustion CO_2 capture acts on the flue gases produced by combustion. CO_2 in these flue gases is diluted (10-15%) and at low pressure (total pressure is ~ 1 bar), which makes CO_2 removal difficult.

The current state-of-the-art post-combustion capture technology is absorption of CO_2 by an aqueous Mono-EthanolAmine (MEA) solution. MEA has a very strong affinity to CO_2 and captures CO_2 efficiently even at low partial pressure but the regeneration of the solvent by heating requires a large amount of energy [1, 2]. Moreover, degradation of the amine by oxygen in the flue gas causes corrosion problems and leads to a high net consumption of solvent (> 1.4 kg MEA/t CO_2 captured, *i.e.* > 4 700 t per year for a 600 MW power plant). Therefore an intensive search for alternative solutions is going on. One of the options is to use Pressure (or Vacuum) Swing Adsorption (PSA or VSA) technology in combination with solid sorbents. PSA/VSA technology is proven and robust, it avoids the difficulties associated with the handling of liquids. The challenge is, however, to find appropriate sorbents. Post-combustion flue gases typically contain 10-15% CO_2, 8-15% H_2O, 3-4% O_2, traces of NO_x and SO_x (depending on the DeNO*x* and DeSO*x* treatment), the balance being N_2. The objective is to capture a high fraction of the CO_2 (90%) and to recover the CO_2 at high purity. The fraction of non-condensable impurities (*i.e.* N_2, O_2) must be below 4% in order to allow the compression of CO_2 for its transport to the storage site. We therefore need highly selective CO_2 sorbents. That is why many amine-based solid sorbents have been studied for post-combustion CO_2 capture [3-9]. Amines can be immobilized on a solid support either by impregnation or by grafting [10]. The acid-base interaction between amino groups and CO_2 assures a very high selectivity towards sorption of CO_2. The presence of water in the flue gas does not interfere with this acid-base interaction. In some cases, the CO_2 capacity is even

enhanced in the presence of water because the formation of bicarbonates becomes possible [11, 12]. Immobilized amines mimic the chemistry of amine based solvents, hence, we find their strengths but also their weaknesses. The strong chemisorption leads to a high CO_2 adsorption capacity at low pressure, the CO_2/N_2 selectivity is quasi infinite but regeneration is rather difficult and degradation may occur. There are also health and safety concerns about the contamination of the decarbonized flue gas by volatilization of the amine or its degradation products.

Another option is the use of physisorbents, like zeolites or Metal Organic Frameworks (MOF). It is well known that polar zeolites like NaX or zeolite 5A are very good adsorbents for CO_2, even at low partial pressures. The adsorption capacity at 0.15 bar is about 3 mol/kg [13], which is comparable to the best amine-based solid sorbents. The CO_2/N_2 selectivity of NaX is also extremely high, above 100 [14]. Similar results are obtained for zeolite 5A [15]. The high capacity and selectivity are a result of the high polarity of the zeolites NaX and 5A. The quadrupole moment of CO_2 strongly interacts with the electric field generated by the extra-framework cations of the zeolite. Metal organic frameworks belonging to the CPO-27 structure type have even higher adsorption capacities than zeolites NaX or 5A under the conditions relevant for CO_2 capture, *i.e.* at a partial pressure of CO_2 of about 0.1 bar [16]. The CPO-27 structure is characterized by the presence of coordinatively unsaturated metal centers, which have a strong affinity for CO_2, similar to the role of the extra-framework cations in zeolites.

A fundamental problem in the design of physisorbents for CO_2 capture is that these materials systematically prefer the adsorption of H_2O over the adsorption of CO_2. Flue gases fatally contain humidity (at low temperatures they are even saturated with humidity). The CO_2 adsorption capacity of NaX, for example, decreases by 99% in humid streams [17], because water is preferentially adsorbed over CO_2. The MOF structures CPO-27-Ni and HKUST-1 are somewhat less sensitive to water than zeolites NaX and 5A but the inhibition of CO_2 adsorption remains very important [16]. Only purely siliceous, defect-free zeolites have been reported to be entirely hydrophobic [18] but these solids are entirely devoid of polarity and therefore have a very low adsorption capacity for CO_2 [19], as well. The dilemma is that a certain polarity of the adsorbent is needed to assure a high adsorption capacity of CO_2 and a high CO_2/N_2 selectivity. Since polarity and hydrophilicity are intimately linked with each other, a high polarity necessarily implies that H_2O will be adsorbed even more strongly and hence strongly inhibit the adsorption of CO_2.

The challenge, therefore, is to tune the polarity of the adsorbent to an intermediate level, so as to find the best compromise between CO_2 adsorption capacity, CO_2/N_2 selectivity, easy of regeneration under vacuum and inhibition by H_2O. Palomino *et al.* [20] nicely demonstrated that the CO_2

adsorption and separation properties can be finely tuned by varying the Si/Al ratio, *i.e.* the polarity, of the framework. In the present study, we have therefore studied the performance of a series of zeolites with varying Si/Al ratios. The adsorption capacity and regenerability of the materials was evaluated by breakthrough experiments with a CO_2/N_2 feed mixture. Also, the water tolerance of the materials was tested. The most promising material was then selected for numerical simulations of a full VSA cycle, in comparison with zeolite NaX.

1 EXPERIMENTAL SECTION

1.1 Adsorbents

The adsorption measurements were carried out on commercial zeolites purchased from Zeolyst *(Tab. 1)*: two mordenites with different Si/Al ratios and two USY zeolites with different Si/Al ratios. Of these four samples, only the CVB10a was in the Na^+ form, the other zeolites have NH_4^+ as extra-framework cation. The NH_4^+ zeolites were transformed into Na^+ zeolites by a three-fold ion exchange with a 0.5 molar solution of NaCl at 363 K. A reference sample of zeolite NaX was provided by CECA.

In addition to the commercial zeolites, a synthetic EMC-1 (FAU-type zeolite) with a Si/Al ratio of 3.9 was tested. This zeolite was prepared according to the recipe described by Chatelain *et al.* [21]. A starting gel having the following molar composition: 10 SiO_2 : 1 Al_2O_3 : 2.1 Na_2O : 0.5 (15-Crown-5) : 100 H_2O was prepared by mixing 55.5 g of 40 wt% silica sol (Ludox HS40, *Dupont*), 6.9 g of sodium aluminate (56% Al_2O_3, 37% Na_2O, *Carlo Erba*), 4.1 g of crown ether (15-crown-5, 98%, *Aldrich*), 2.56 g of sodium hydroxyde (98%, *Fluka*) and 30.9 g of water (desionized water, 18 MΩ). This zeolite was synthesised hydrothermally

TABLE 1

Global and framework Si/Al ratio, Na-content, surface area and micropore volume of the samples

Sample	Si/Al	Si/Al$_f$	Wt% Na	S$_{BET}$ (m²/g)	V$_{micro}$ (cm³/g)
Na-MOR-6 (CBV10a)	6.2	8	4.8%	415	
NH₄-MOR-10 (CBV21a)[a]	10		0.06%	424	0.17
Na-MOR-10			2.78%		
NH₄-USY-6 (CBV712)[a]	6	11	0.04%	791	0.27
Na-USY-6			1.3%		
NH₄-USY-15 (CBV720)[a]	15.2	25	0.02%	805	0.25
Na-USY-15			1.07%		
EMC-1	3.9		6.02%	780	0.33
NaX	1.3	1.3	9.68%	816	0.34

[a] NH₄-zeolites are transformed into H-zeolites by thermal activation before testing.

in a 100 mL stainless steel autoclave at 110°C for 8 hours. After cooling to room temperature, the crystals were filtered on a Buchner funnel, and washed thoroughly with deionized water. The products were dried overnight at 100°C and calcined at 550°C under air during 8 hours.

The Si/Al ratio of the zeolites was determined by X-ray fluorescence. The USY zeolites contain quite a high fraction of extra-framework Al. The actual framework Si/Al ratio was therefore estimated from ^{29}Si-NMR and IR spectroscopy. The Na-content of the materials was determined from atomic absorption spectroscopy.

The porosity of the adsorbents was characterized by their N_2 adsorption isotherm at 77 K (measured on a Micromeretics ASAP 2010). BET surface areas and micropore volumes (obtained from a t-plot) are compiled in Table 1.

1.2 Breakthrough Experiments

The adsorbents were filled into a column that was placed into an oven. A gas distribution system allowed us to feed the column either with pure N_2 or with a mixture of CO_2 in N_2 and to switch rapidly between the two. Moreover, we had the possibility to introduce water vapour into the feed stream by passing *via* a saturator. The pressure was always atmospheric plus the (small) pressure drop over the column (between 0.1 and 1 bar, depending on the adsorbent). The sorbents were initially treated in N_2 at 623 K for 2 h and then brought to the adsorption temperature (323 K) and a breakthrough curve $N_2 \rightarrow N_2 + CO_2$ was recorded by means of a TCD detector at the column exit. Adsorption isotherms of CO_2 were measured by repeating the breakthrough experiments at different CO_2 concentrations (from 5 to 30%), each time followed by a regeneration at 623 K for 2 h. Note that these isotherms are in fact CO_2/N_2 co-adsorption isotherms but the amount of adsorbed N_2 is not quantified. In addition to the adsorption isotherms, cyclic adsorption-desorption experiments were performed. In that case, the CO_2 concentration was fixed at 15% and the feed was alternated between $CO_2 + N_2$ and N_2, while keeping the temperature constant. These cyclic adsorption experiments give us information on the regenerability of the samples.

For evaluating the influence of humidity on adsorption, the following procedure was used. The N_2 stream was passed through a saturator that was filled with distilled water and thermostated at 306 K (which corresponds to a vapour pressure of 5 kPa) for 1 h before starting the breakthrough experiment. During the whole breakthrough experiment the partial pressure of H_2O was maintained at 5 kPa by passing through the saturator. At the column exit water was condensed in a cool bath (at 273 K) so as to enter with a gas of constant humidity into the TCD detector. After breakthrough the feed was switched back to humid N_2 and the breakthrough experiment with humid feed was repeated at intervals of several hours.

Breakthrough experiments for measuring the CO_2/N_2 selectivity were carried out on a different experimental setup. Activation was carried out in a non-adsorbable carrier gas (He) and the breakthrough curve was triggered by switching from He to a 50/50 mixture of CO_2/N_2. The CO_2 and N_2 concentrations at the column exit were measured by a mass spectrometer, following the procedure described in [22]. The experiments were carried out at 303 K. At least four breakthrough/desorption measurements were carried out with each adsorbent:

– a step from He to CO_2/N_2, followed by a step back to He;
– a step from pure CO_2 to CO_2/N_2, followed by a step back to He.

The adsorbed amount of CO_2 was determined from the step He → CO_2/N_2, the amount of N_2 was obtained by averaging the results of the four breakthrough/desorption curves. For an equimolar feed mixture of CO_2/N_2 the adsorption selectivity α simply corresponds to the ratio of the adsorbed amounts of CO_2 and N_2.

2 RESULTS

2.1 Adsorption Isotherms

Figure 1 compares the adsorption isotherms of CO_2 over three different mordenite samples. It clearly shows the influence of Si/Al ratio and of the extra-framework cation on the adsorption properties. The sample with the lower Si/Al ratio has the higher adsorption capacity. Moreover,

Na^+-exchanged samples adsorb more CO_2 than H-mordenite (activation transforms NH_4-mordenite into H-mordenite). It has already been shown before that Na-ZSM-5 has a higher heat of adsorption than H-ZSM-5 [23]. The electrostatic interaction between the Na^+ cations and the quadrupole moment of CO_2 is stronger than that of a largely covalent Bronsted OH-group.

The trends observed for mordenite are confirmed with the faujasite adsorbents *(Fig. 2)*. The CO_2 adsorption capacity decreases with increasing Si/Al ratio and NH_4-exchanged samples adsorb much less CO_2 than Na-faujasites. Zeolite NaX has by far the highest adsorption capacity because its Si/Al ratio is much lower than that of the other faujasites. At similar Si/Al ratio, the CO_2 isotherms of the Na-faujasite samples are not as steep as the isotherms of Na-mordenites. The strong initial adsorption of CO_2 in mordenite may be related to the strong confinement in the side pockets of the mordenite structure.

In order to rationalize the adsorption data on the series of faujasite and mordenite samples, the isotherms were fitted by a Langmuir model:

$$q = q_{sat} \cdot \frac{b \cdot p_{CO_2}}{1 + b \cdot p_{CO_2}}$$

The Henry constants of the isotherms were then calculated from $K_{Henry} = b \times q_{sat}$.

Figure 3 shows that the Henry constants are correlated with the Na content of the zeolites, which indicates that the Na^+ cations are the preferred adsorption sites of CO_2. The Na content can, therefore, be regarded as a good semi-quantitative indicator of the polarity of the zeolite. The slope of the curve
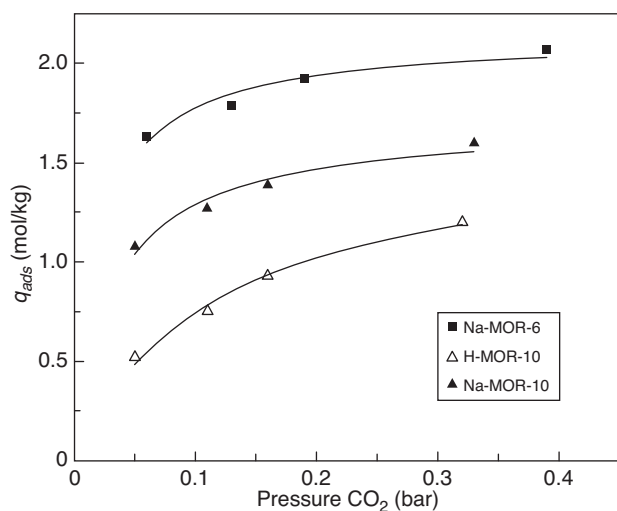

Figure 1

Adsorption isotherms of CO_2 (in mixture with N_2) at 323 K over three different mordenite samples.
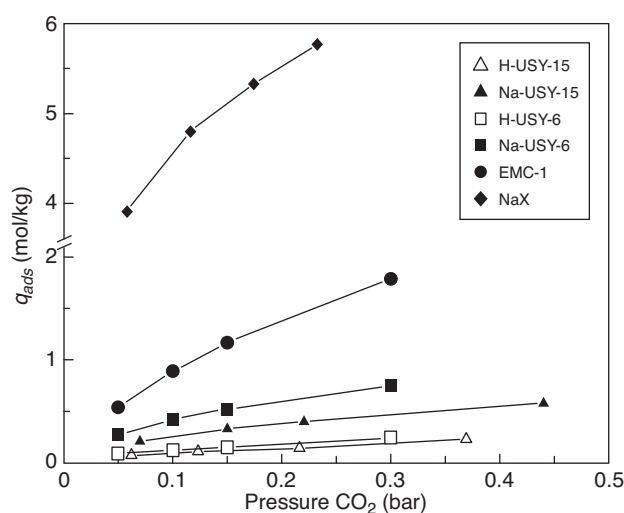

Figure 2

Adsorption isotherms of CO_2 (in mixture with N_2) at 323 K over different faujasite samples.
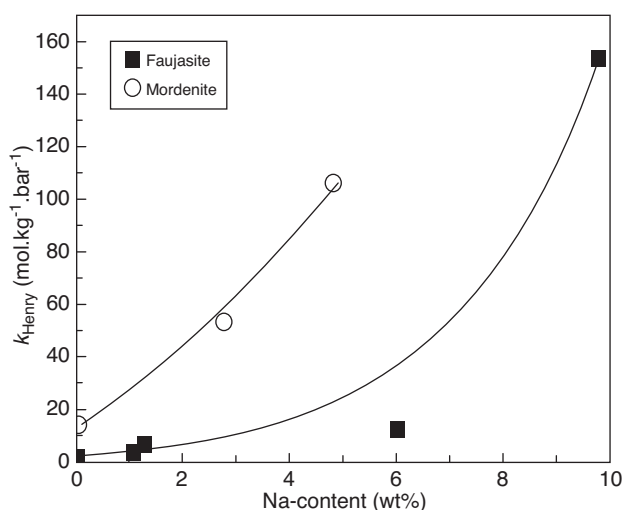
Figure 3

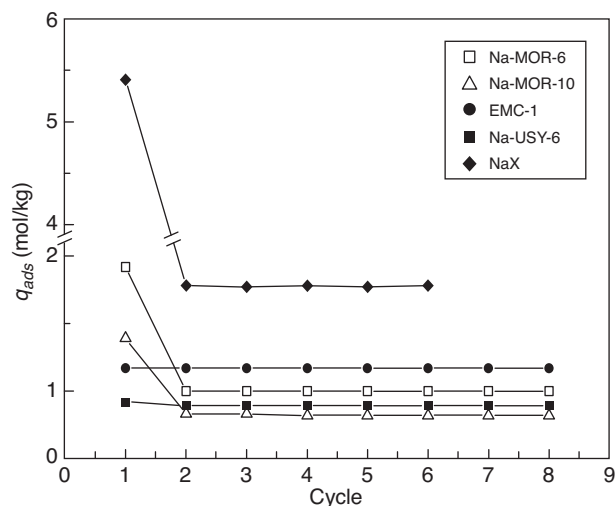Henry constants of the CO_2 isotherms at 323 K as a function of the Na content of the zeolites.

Figure 4

Adsorption capacity over several adsorption-desorption cycles at 323 K. CO_2 concentration 15% in N_2, desorption by N_2 purge for 30 min.

K_{Henry} *vs* Na-content is much higher on mordenite than on faujasite. In mordenite, the electrostatic effect of the Na^+ cations is exacerbated by a stronger confinement, *i.e.* a smaller pore size.

2.2 Adsorption — Desorption Cycles

A high adsorption capacity at the working pressure of the process is not a sufficient criterion for the selection of an adsorbent. The adsorbent must also be easily regenerable

upon depressurisation and desorption under vacuum. The quantity that can be adsorbed and desorbed over many adsorption/desorption cycles is called the working capacity of the adsorbent. Since our experimental setup did not allow us to regenerate the adsorbents under vacuum, we established a qualitative ranking of their regenerability, by desorbing CO_2 *via* a N_2 purge gas for 30 min at 323 K (*i.e.* under isothermal conditions). The results are shown in Figure 4. With the exception of NaX, the faujasite adsorbents were perfectly regenerable by the N_2 purge and the adsorption capacity remained constant during 8 adsorption/desorption cycles. The two Na-mordenites lost a significant fraction of their initial adsorption capacity when going from the 1st to the 2nd cycle, *i.e.* they were not fully regenerable by a N_2 purge. Also in the case of NaX, 30 min were largely insufficient to desorb CO_2 from the column. As expected, the regenerability was related to the shape of the isotherm at low pressure. Very steep isotherms (*i.e.* NaX, Na-MOR-6, Na-MOR-10) mean difficult regeneration. In spite of its bad regenerability, the best cyclic capacity was obtained with NaX (1.8 mol/kg), followed by EMC-1 (1.2 mol/kg).

2.3 CO₂/N₂ Selectivity

The CO_2/N_2 selectivity was measured by breakthrough experiments with 50/50 mixtures of CO_2/N_2.

Figure 5 compares the breakthrough curves of EMC-1, Na-USY-15 and Na-MOR-10. One can immediately see that the quality of the CO_2/N_2 separation was less good on Na-USY-15. The selectivity values are reported in Table 2[1]. Both Na-mordenites as well as NaX and EMC-1 had selectivities above 40 (all selectivities above 40 were considered to be equal because of the large experimental error). In the case Na-USY-15, which is the least polar sample that was tested, the selectivity dropped significantly to 11. This suggests that there is a minimum polarity above which there is no measureable gain in the CO_2/N_2 selectivity any more. For faujasite samples, this threshold is somewhere between Na-USY-15 and EMC-1.

TABLE 2

Results of breakthrough experiments of a 50/50 CO_2/N_2 mixture at 303 K

	Q_{ads} CO_2 (mol/kg)	Q_{ads} N_2 (mol/kg)	Selectivity
NaX	5.46	0.10 ± 0.04	54 ± 22
EMC-1	2.84	0.06 ± 0.03	44 ± 22
Na-USY-15	1.16	0.11 ± 0.03	11 ± 3
Na-MOR-6	3.23	0.08 ± 0.04	42 ± 25
Na-MOR-10	2.42	0.03 ± 0.01	80 ± 30

[1] The adsorbed amount of N_2 is very small. We, therefore, averaged results from several tests to obtain fairly reliable results.
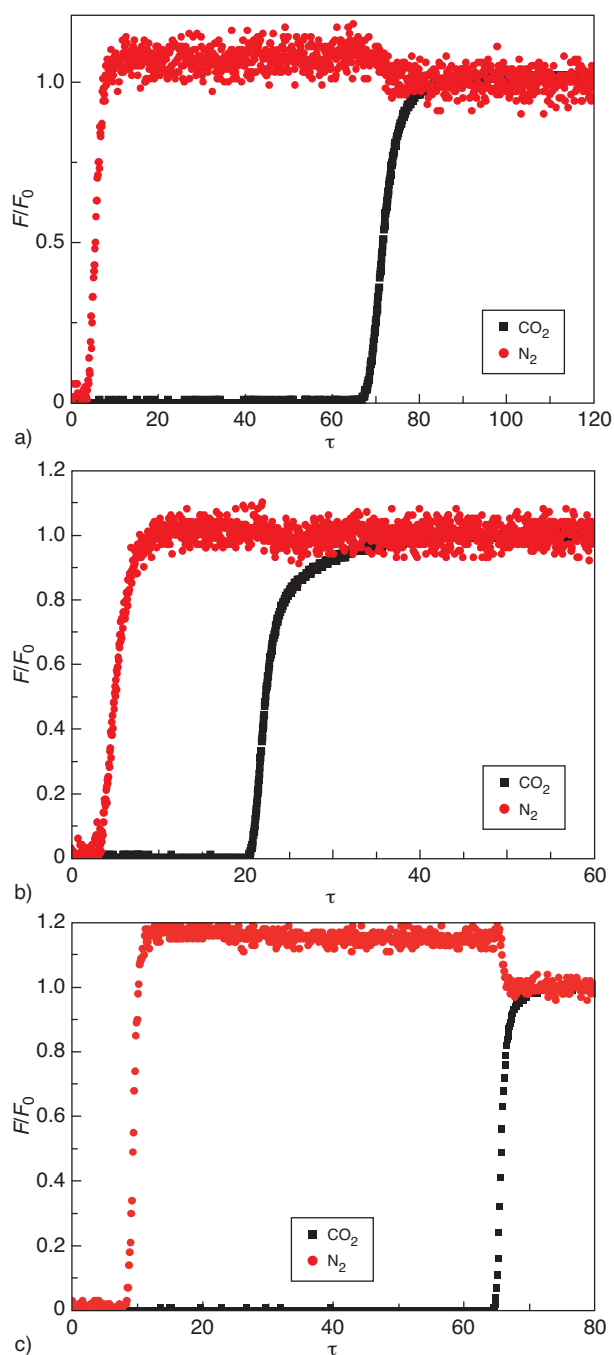
a)

b)

c)

Figure 5

Breakthrough curves of a 50/50 mixture of CO_2/N_2 over a) EMC-1, b) Na-USY-15, c) Na-MOR-10. F/F_0 = normalized molar flow rate at column exit (F_0 = feed flow rate). τ = time/contact time.

2.4 Inhibition by H$_2$O

As a next step, we evaluated the effect of humidity on CO_2 adsorption. Breakthrough experiments were carried out with humid gases, *i.e.* by switching from a mixture $N_2 + H_2O$ to a
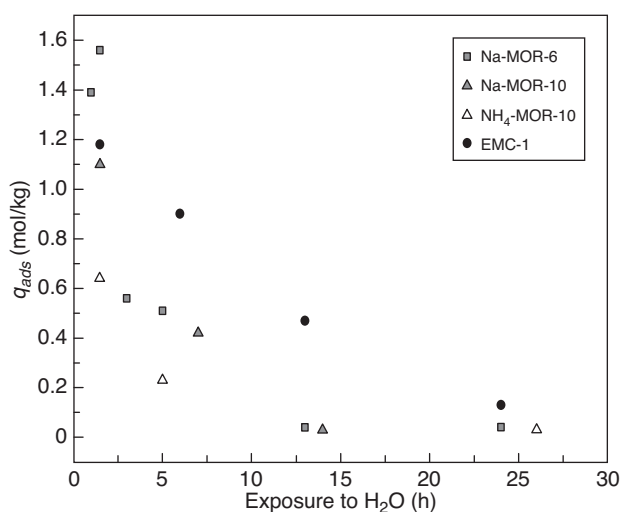
Figure 6

CO_2 adsorption capacity in a humid feed (15% CO_2, 5% H_2O) as a function of the total exposure time of the adsorbent to a humid gas.

mixture of $N_2 + CO_2 + H_2O$. The H_2O content was regulated by a saturator, which was thermostated at 306 K. This corresponds to a vapor pressure of 0.05 bar and a relative humidity of 43% at 323 K. The adsorbent was exposed to the $N_2 + H_2O$ mixture for 1 h before adding CO_2 to the feed. For the three mordenite samples, the CO_2 adsorption capacity dropped by 0.3 mol/kg compared to a dry feed. For EMC-1, no significant change was observed. We noticed, however, that the CO_2 capacity dropped more strongly when the initial exposure to the $N_2 + H_2O$ mixture was prolonged *(Fig. 6)*. That made us suspect that the solids were not yet saturated with H_2O. We therefore carried out several successive breakthrough experiments, at increasing total exposure times to H_2O. Figure 6 shows that the CO_2 adsorption capacity rapidly decreases with increasing exposure time to humid feed. Already after 15 h of exposure to 5% H_2O, the adsorption capacity of CO_2 has dropped almost to zero. 10 h corresponds roughly to the time needed to saturate the pore volume of mordenite with water under our conditions (concentration and flow rate). We can deduce that the pore volume of mordenite is indeed gradually filled with H_2O. As soon as the whole column is saturated with H_2O hardly any CO_2 can be adsorbed any more. In the case of EMC-1, the CO_2 adsorption capacity decreases more gradually, which is probably due to the higher of pore volume of EMC-1, *i.e.* it takes more time to fill the pores with H_2O but the principle remains the same.

These results confirm that even zeolites with moderate polarity like H-MOR-10 largely prefer the adsorption of H_2O over the adsorption of CO_2. This does not mean that it is impossible to run a CO_2 adsorption process with zeolites in the presence of H_2O but a large part of the bed will be

monopolized by the adsorption of H_2O and not be effective at all for CO_2 capture. Since water has a very strong affinity for zeolites its regeneration will be very difficult. It makes more sense to remove the bulk of the water content by "weaker" adsorbents, like silica gel, alumina or activated carbons [24].

3 MODELING OF THE VSA CO$_2$ CAPTURE PROCESS

After having presented the adsorption properties of a series of zeolites, we now turn to the chemical engineering aspects of a CO_2 capture process by VSA. We first discuss the technical boundary conditions, then describe the numerical modeling of the VSA process and finally discuss the industrial feasibility of CO_2 by VSA.

3.1 Boundary Conditions

Any process for CO_2 capture from flue gases must fulfill two technical targets:
– achieve a high CO_2 recovery;
– produce a CO_2 of high purity that is suited for sequestration.

The optimum recovery level is defined by the trade-off between recovery and cost, *i.e.* by minimizing the price of avoided CO_2. The energy consumption (per captured CO_2) of a VSA process increases with increasing recovery (as will be discussed later). On the other hand, the capital expenses for constructing a CO_2 capture plant do not depend much on the recovery and will, therefore, contribute more heavily to the overall cost, when the recovery is low. Many studies consider a recovery level of 90%, so we started out by fixing our target recovery to this value.

The technical constraint in terms of purity of the CO_2 is stricter. The level of non-condensable impurities, *i.e.* N_2 and O_2, must be below 4% in order to facilitate the compression of CO_2 to a supercritical state, for the purpose of transport and sequestration.

Purity strongly depends on the selectivity of the adsorbent. At the end of the adsorption step, some N_2 (and O_2) is co-adsorbed on the zeolite and some is present in the interstitial volume of the bed. In order to achieve 96% purity, a large fraction of the N_2 must be removed from the bed before the CO_2 recovery step. This can be achieved by modifications of the VSA cycle [25-28]. A co-current depressurisation of the bed, at the end of the adsorption step, releases a large fraction of the N_2 from the interstitial volume and allows advancing the concentration front of CO_2 towards to end of the bed, without sacrificing recovery, since the effluent of the depressurisation step is recycled for repressurisation of another bed. Additionally, a CO_2 rinse step, in which part of the recovered CO_2 is recycled to the bed, may be added in order to displace co-adsorbed N_2 from the adsorbent. Depressurisation and CO_2 rinse may be combined. The lower the pressure of the CO_2 rinse step P_R is chosen, the smaller is the amount of CO_2 required for purging the column and the smaller is the energy consumption for compressing the CO_2 recycle stream to P_R. In order to maintain a high recovery of CO_2, the effluent of the depressurization step is usually used to repressurize another column to an intermediate pressure P_I (*Fig. 7*). In that case, the condition $P_R > P_I$ puts an upper limit on the amount of gas that can be used for repressurization, which indirectly imposes a lower limit on P_R.

After having removed a large fraction of N_2 and O_2 from the column by depressurization and purge, CO_2 is recovered by lowering the pressure, *i.e.* by pulling vacuum. In conventional PSA processes, the column is further regenerated
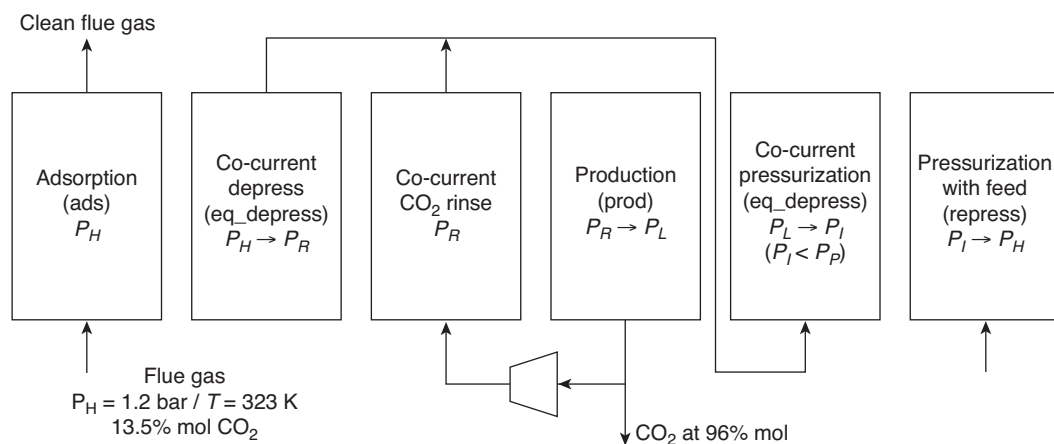

Figure 7

VSA cycle for CO_2 capture from flue gas.

by a purge with the light product, so as to perfectly clean the light product end of the column but, in the present case, it is not possible to employ a purge with a non-condensable gas like N_2 (*vide infra)*, because of the stringent purity requirements in CO_2 capture. Therefore, at the end of the CO_2 recovery step, the light product end of the column is in equilibrium with almost pure CO_2 at the partial pressure of regeneration (plus the pressure drop in the column). In the following adsorption step, CO_2 cannot be adsorbed beyond that equilibrium partial pressure, leading to a permanent slip of CO_2 that limits the recovery. For example, if the adsorption is carried out at a pressure of 1.2 bar and the CO_2 concentration is 15%, the pressure of regeneration must be below 0.018 bar in order to be able to achieve a recovery of 90%. An examination of earlier simulation and experimental work on VSA for CO_2 capture confirms that recovery is limited by the ratio between the partial pressures of CO_2 in the feed step and in the regeneration step [29, 30], if the column is not purged with light product.

In order to be able to circumvent the use of such low pressures for regeneration, one would have to find another way to clean the light product end of the bed before starting a new adsorption step. Many VSA simulation studies employ a low pressure purge with light product (N_2) but, as already mentioned above, a N_2 purge necessarily pollutes the CO_2 product and makes it impossible to achieve the 96% purity [27, 28, 31]. An alternative is to repressurize the column from the light product end with N_2 (instead of repressurizing with feed). This method can be effective for adsorbents with a low CO_2/N_2 selectivity, like activated carbons. On an activated carbon N_2 competes with CO_2 for adsorption sites and a repressurization by N_2 can push the concentration front of CO_2 back into the column [32]. In polar zeolites, the co-adsorption of N_2 is very weak, as a consequence repressurizing with N_2 hardly affects the CO_2 concentration front. It is therefore impossible to avoid the very low regeneration pressures in VSA cycles with highly selective adsorbents. Since recovery is intimately related to the regeneration pressure and since the power consumption of the VSA process increases with decreasing regeneration pressure, we can now understand why a higher recovery leads to higher operating costs.

3.2 VSA Simulations

From our experimental screening of zeolites, two materials emerged as the most attractive candidates for a CO_2 capture application: zeolite NaX has a very high CO_2 affinity and a high adsorption capacity but is difficult to regenerate; zeolite EMC-1 has a moderate adsorption capacity but exhibits excellent regenerability. Both have a high CO_2/N_2 selectivity. We have, therefore, decided to confront the behavior of EMC-1 and NaX in a VSA cycle by numerical simulations. The flue gas was represented by a mixture of 13.5% CO_2 in N_2. For the sake of simplicity, a dry feed was used, *i.e.* it was

assumed that water has been removed from the flue gas upstream of the VSA. The single component adsorption isotherms of CO_2 and N_2 on NaX were taken from the literature [23], the isotherms of EMC-1 were in-house data. The experimental isotherms were modeled by a dual or single site Langmuir model:

$$q_j = \sum_i q_{sat,j} \cdot \frac{b_{j,i} \cdot p_j}{1 + b_{j,i} \cdot p_j}$$

$$b_{j,i} = b_{j,i,0} \cdot \exp\left(\frac{-h_{ads,j,i}}{RT}\right)$$

The parameters are given in Table 3.

TABLE 3

Parameters of the single or dual site Langmuir model used to fit the experimental isotherms of CO_2 and N_2

		q_{sat} (mol/kg)	b_0 (Pa^{-1})	h_{ads} (kJ/mol)
NaX	CO_2	2.09	3.84×10^{-10}	-40
		4.11	8.75×10^{-12}	-40
	N_2	6.25	3.81×10^{-10}	-19
EMC-1	CO_2	3.34	3.24×10^{-9}	-25
		4.15	4.70×10^{-10}	-25
	N_2	3.81	4.35×10^{-10}	-18

A simple extended Langmuir equation was used for modeling the co-adsorption of CO_2 and N_2:

$$q_j = q_{sat,j,1} \cdot \frac{b_{j,1} \cdot p_j}{1 + \sum_m b_{m,1} \cdot p_m} + q_{sat,j,2} \cdot \frac{b_{j,2} \cdot p_j}{1 + \sum_m b_{m,2} \cdot p_m}$$

This is not the most precise co-adsorption model but is sufficiently accurate for a qualitative comparison of NaX and EMC-1. Since we were mainly interested in identifying the effect of the adsorption isotherms on the performance, we chose conditions under which mass transfer effects are totally negligible, *i.e.* a fairly long contact time of 0.4 s. The maximum gas velocity was fixed *via* the constraint of avoiding fluidization of the adsorbent particles and the column height was limited by the pressure drop (which should be below 0.2 bar). The adsorber column was considered to be adiabatic and the pressure drop in the column was neglected in the simulation. Further details of the model and its underlying assumptions are given in the Appendix. The VSA cycle was chosen based on the considerations above: an adsorption step, at $P_H = 1.2$ bar (to overcome the pressure drop in the column) and 323 K was followed by a co-current depressurization to P_R. The objective of the depressurization step was to remove N_2 from the interstitial volume of the column. The depressurization was followed by a rinse with part of the recovered CO_2 stream. In the next step, CO_2 was produced by lowering

the pressure to P_L, *i.e.* by pulling vacuum on the column. Part of the CO_2 that is recovered during this step is recycled to another column, for performing the CO_2 rinse. For this purpose, CO_2 must be compressed from P_L to P_R. Finally the column is repressurized, first with effluent of a column in depressurization and finally with the feed.

The most influential operating parameters of the VSA cycle were:

- the value of P_L: as explained above, it had a huge influence on recovery;
- the value of P_R: it had a large influence on the purity of CO_2;
- the duration of the adsorption and rinse steps.

These four parameters were varied in order to achieve our target values of 90% recovery and 96% purity. We found that, thanks to the high selectivity of NaX and EMC-1, a CO_2 rinse step was actually not necessary. The 96% purity of CO_2 could be achieved simply by optimizing the final pressure of the depressurization step.

Table 4 shows the conditions under which the target recovery and purity were achieved for NaX and EMC-1. The values of the key parameters t_{ads}, P_P and P_L, were surprisingly close for the two materials. As a consequence, productivity and power consumption for the evacuation step were also quite similar. The working capacities, *i.e.* the amounts of CO_2 adsorbed in each cycle, were 0.70 and 0.75 mol/kg for NaX and EMC-1, respectively. Remember that our screening experiments had yielded cyclic capacities of 1.8 and 1.2 mol/kg for NaX and EMC-1, respectively. Two factors may degrade the working capacity in the VSA simulations compared to the cyclic capacity obtained in our screening. First of all, temperature rise in adsorption and the temperature drop in desorption diminishes the capacity of the bed compared to isothermal operation. Secondly, the equilibrium capacity of the bed is not fully exploited because the mass transfer zone of CO_2 must be contained in the bed in order to achieve a high recovery of CO_2.

In order to evaluate the importance of these two effects, we have calculated the theoretical working capacity at equilibrium, first under isothermal and then under adiabatic conditions. For calculating the theoretical isothermal working capacity, we assumed that the whole adsorbent is in equilibrium with $P_H \times 0.135 = 0.16$ bar CO_2 and with $P_L = 0.014$ bar CO_2 at the end of the adsorption step and of the desorption step, respectively. The difference between these two equilibrium adsorbed amounts yielded the theoretical working capacity. The theoretical capacities were 1.7 and 1.3 mol/kg for NaX and EMC-1, respectively, *i.e.* close to the experimental cyclic capacities *(Tab. 5)*. Co-adsorption of N_2 had a negligible impact on the theoretical working capacity. The good agreement between theoretical and experimental working capacities implies that our screening method was pertinent. As a next step, the adsorption isotherms were transposed into an adiabates [33], by accounting for the temperature rise caused by the exothermicity of adsorption, and the associated decrease of the adsorption capacity. For calculating the theoretical adiabatic working capacity, we assumed that the whole adsorbent is in equilibrium with $P_H \times 0.135 = 0.16$ bar CO_2 at 323 K + $\Delta T/2$ at the end of the adsorption step, and that the whole adsorbent is in equilibrium with $P_L = 0.014$ bar at 323 K – $\Delta T/2$. ΔT is the temperature swing between adsorption and desorption. The adiabatic capacities were 0.7 and 0.9 mol/kg for NaX and EMC-1, respectively. The working capacity of NaX dropped by 60% when the thermal effects were taken into account. The impact of adiabatic operation on the working capacity of EMC-1 was much smaller because its heat of adsorption is lower. The VSA simulations confirmed that the temperature swing between adsorption and desorption was indeed higher in the case of NaX *(Fig. 8)*.

TABLE 5

Working capacities of NaX and EMC-1: experimental estimation by adsorption – desorption experiments, theoretical calculation under isothermal and adiabatic conditions and values obtained in the VSA simulations

Working capacity (mol/kg)	NaX	EMC-1
Experimental screening	1.8	1.2
Theoretical isothermal	1.75	1.35
Theoretical adiabatic	0.7	0.9
VSA simulations	0.7	0.75

TABLE 4

Results of the simulations of a VSA cycle for CO_2 capture, using either NaX or EMC-1 as adsorbent

	NaX	EMC-1
$t_{ads}^{(a)}$ (s)	450	480
P_P (bar)	0.55	0.4
P_L (bar)	0.014	0.015
Purity CO_2	96.7%	95.9%
Recovery CO_2	89.9%	89.8%
Power consumption[(b)] (kJ/mol CO_2)	11.7	11.0

[a] Feed rate = 60 000 Nm³/h, column volume = 25.13 m³.
[b] Power consumption during the CO_2 production step.

The theoretical adiabatic working capacities were fairly close to the simulated working capacities, which means that they are a good qualitative indicator of the performance of an adsorbent. Still, the theoretical values predict that EMC-1 should perform slightly better than NaX in adiabatic operation, but in the VSA simulations both solids were equivalent. The explanation can be found in the concentration profiles *(Fig. 9)*.
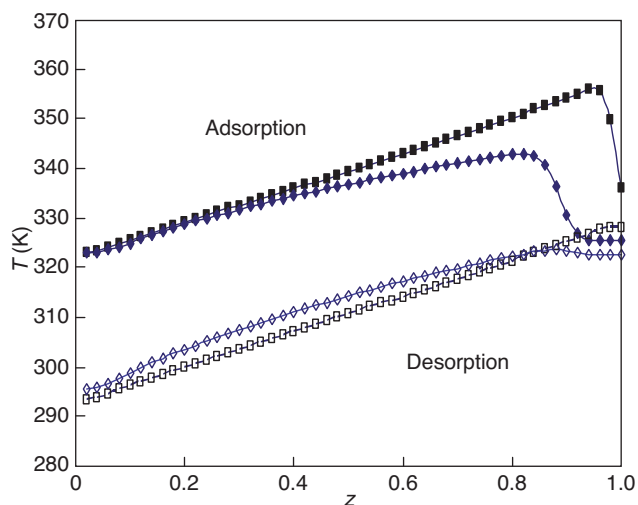
Figure 8

Temperature profile along the column axis z (adimensionalized) at the end of the adsorption step (full symbols) and at the end of the desorption step (empty symbols). NaX (squares) *vs*. EMC-1 (diamonds).

The mass transfer zone in the EMC-1 column was significantly larger than in the NaX column, *i.e.* the capacity of the bed was less well exploited. The CO_2/N_2 co-adsorption isotherm of EMC-1 is less favorable than that of NaX and this leads to a stronger dispersion of the CO_2 concentration front at low concentrations.

In summary, the moderate CO_2 affinity of EMC-1 compared to NaX was an advantage, because it diminished the temperature excursions in the column and therefore led to a higher theoretical working capacity under adiabatic conditions. In practice part of this advantage was lost, because the less favorable CO_2 isotherm of EMC-1 led to a broader mass transfer zone, hence the bed was less well exploited. Overall, the effects cancelled each other and the performance of both solid was quasi equivalent. In practice, one would probably stick with NaX as the preferred adsorbent since its preparation is easier and cheaper.

3.3 Industrial Feasibility

The major asset of VSA technology for CO_2 capture is the fact that the energy consumption of process is, at least theoretically, very low. According to our simulations under idealized conditions, *i.e.* under total absence of mass transfer limitations, the power consumption of the vacuum pump and the blower used for compressing the feed to 1.2 bar amounts to only 0.35 GJ/t CO_2. This theoretical value is lower than recently published estimates (also based on simulation data) [27], because in our case a high recovery and purity of CO_2 could be achieved without using a CO_2 rinse step (the recycling
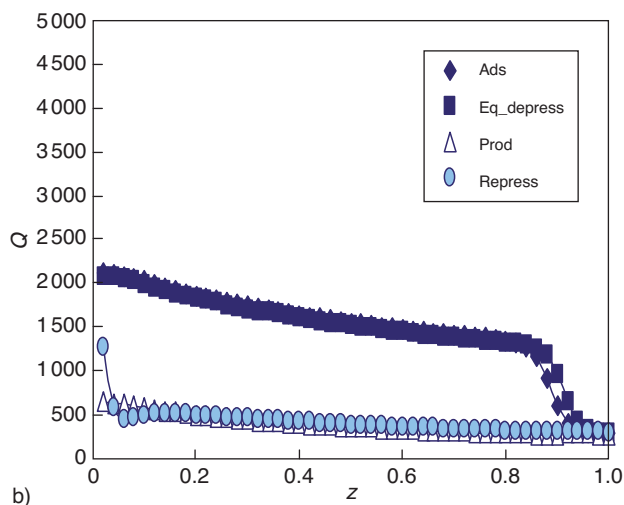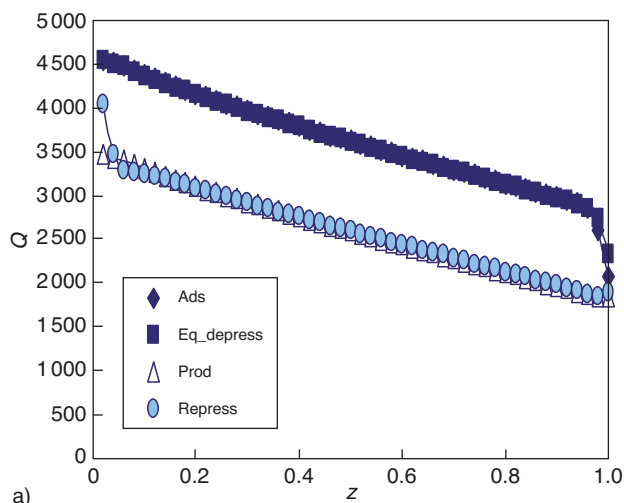

Figure 9

Axial concentration profiles of CO_2 in the adsorbed phase Q (in mol/m³crystal) at the end of the different steps of the cycle: ads = adsorption, eq_depress = co-current depressurization, prod = production of CO_2, repress = repressurization with fedd. a) NaX (squares), b) EMC-1 (diamonds).

of CO_2 consumed additional energy). Yet, the simulated theoretical values are overly optimistic because they assume a 100% efficiency of the (vacuum) blowers. Experimentally measured energy consumptions are a factor of 4-5 higher than the theoretical values [34, 35]. Moreover, one has to be careful when comparing the electrical energy used by blowers with thermal energy used in temperature swing processes, as absorption by MEA. Electrical energy is produced from thermal energy with an efficiency of ~40%, it is therefore more "expensive". When both of these factors are taken into account, the energy balance of the VSA process is not that favorable any more.

In addition, application of the VSA technology on a large scale (*i.e.* the scale required for a 600 MW power plant) faces serious technological problems, which are rarely taken into account in the literature. The flue gas flow rate in a 600 MW power plant is in the order of 1.8×10^6 Nm^3/h. In order to be able to treat this enormous flow rate, while keeping the pressure drop over the column low, huge cross sections are needed. If we extrapolate our simulations to the above-mentioned feed flow rate, the total cross section of the adsorbers should be 1 500 m^2. The actual value should be lower because we carried out our simulations at fairly low gas velocities so as to avoid any mass transfer limitation. For comparison, Lively *et al.* [36] estimated the cross section of fixed bed adsorbers to be 850 m^2, if a pressure drop of 0.69 bar is authorized. These huge cross sections ask for new concepts in adsorber design, for example, structured adsorbent beds, where the adsorbents are packed into hollow fibers [34, 36, 37]. Such solutions are not yet industrial standard.

Another concern that must be raised about CO$_2$ capture by VSA is the very low pressure that must be used for desorption of CO$_2$ in order to assure a high recovery (see above). At 0.014 bar, the volume flow rate of the recovered CO$_2$ stream is 10 times higher than the volume flow rate of the feed. A large number of pumps must be installed in parallel in order to be able to cope with this huge volume flow and several compression stages are probably needed to raise the pressure of the recovered CO$_2$ stream back to 1 bar (pressure at which CO$_2$ is released in the reference MEA process). The high capital expenses associated with the installation of a large number of blowers, as well as the technological difficulty of dealing with the huge volume flow rates encountered during CO$_2$ recovery may render CO$_2$ capture by VSA processes economically unviable. A way to circumvent to low pressure desorption is to use dual-reflux systems [38-41]. In dual-reflux pressure swing separations, the feed is injected at an intermediate point of the column. Light product (N$_2$) is recycled to the top of the column and heavy product (CO$_2$) is recycled to the bottom of the column. In this way, both light and heavy product can be obtained at high recovery and purity, at desorption pressures as high as 0.3 bar [38, 41]. We are, however, not aware of any existing industrial unit that has been constructed according to a dual-reflux design.

CONCLUSIONS

One of the objectives of the present work was to tune the adsorption properties of zeolites so as to optimize their performance in post-combustion CO$_2$ capture. Our results show that it is possible to modulate the CO$_2$ adsorption isotherms of zeolites by changing the content of extra-framework Na$^+$ cations and/or the zeolite structure (*i.e.* the pore size and pore geometry). Within a given zeolite structure, reducing the extra-framework cation content reduces the adsorption

capacity at low pressure but improves the regenerability. The CO$_2$/N$_2$ selectivity is not measurably affected as long as the Na$^+$ content is above a certain threshold (which is around 2% wt Na for faujasite zeolites). Among the series of faujasite and mordenite zeolites that we have tested, the faujasites NaX (Si/Al = 1.3) and Na-EMC-1 (Si/Al = 3.9) present the best working capacity in cyclic adsorption – desorption experiments. Zeolite NaX has a very high CO$_2$ affinity, a high heat of adsorption and a high adsorption capacity but is difficult to regenerate; zeolite EMC-1 has a moderate adsorption capacity (and a moderate heat of adsorption) but exhibits excellent regenerability. Both solids exhibit a high CO$_2$/N$_2$ selectivity. Under isothermal conditions, the working capacity of zeolite NaX is about 50% higher than that of zeolite EMC-1. In adiabatic operation, the ranking is inversed. The higher heat of adsorption of CO$_2$ on NaX (compared to EMC-1) leads to higher temperature excursions in the bed during adsorption and desorption, and thereby strongly degrades the adsorption capacity of NaX [25, 26], even below the value of EMC-1. Simulations of a VSA cycle for CO$_2$ capture show, however, that the small theoretical advantage of EMC-1 is lost because the less favorable CO$_2$ isotherm of EMC-1 leads to a broader mass transfer zone, hence the bed is less well exploited.

From an application point of view, the main asset of VSA technology for CO$_2$ capture is the fact that the energy consumption of the process could, at least theoretically, be very low. There are, however, many technological hurdles to be overcome before VSA for CO$_2$ capture can become an industrial reality. Vacuum blowers are needed that can cope with huge volumetric flow rates and adsorber design has to be reinvented in order to minimize the pressure drop in the system. An additional obstacle is that the flue gas must be dried within or upstream of the VSA system, because all of the most promising CO$_2$ adsorbents largely prefer the adsorption of H$_2$O over the adsorption of CO$_2$. It is, therefore, highly uncertain whether CO$_2$ capture by VSA technology for large scale power plants can be economically and technically viable in the near future.

REFERENCES

1 Raynal L., Bouillon P.A., Gomez A., Broutin P. (2011) From MEA to demixing solvents and future steps, a roadmap for lowering the cost of post-combustion carbon capture, *Chem. Eng. J.* **171**, 3, 742-752.

2 Knudsen J.N., Jensen P.J., Vilhelmsen P.J., Biede O. (2009) Experience with CO$_2$ capture from coal flue gas in pilot-scale: Testing of different amine solvents, *Energy Procedia* **1**, 783-790.

3 Serna-Guerrero R., Belmabkhout Y., Sayari A. (2010) Further investigations of CO_2 capture using triamine-grafted pore-expanded mesoporous silica, *Chem. Eng. J.* **158**, 3, 513-519.

4 Serna-Guerrero R., Belmabkhout Y., Sayari A. (2010) Triamine-grafted pore-expanded mesoporous silica for CO_2 capture: Effect of moisture and adsorbent regeneration strategies, *Adsorption* **16**, 6, 567-575.

5 Belmabkhout Y., Sayari A. (2010) Isothermal *versus* Non-isothermal Adsorption-Desorption Cycling of Triamine-Grafted Pore-Expanded MCM-41 Mesoporous Silica for CO_2 Capture from Flue Gas, *Energy Fuels* **24**, 5273-5280.

6 Drese J.H., Choi S., Lively R.P., Koros W.J., Fauth D.J., Gray M.L., Jones C.W. (2009) Synthesis-Structure-Property Relationships for Hyperbranched Aminosilica CO_2 Adsorbents, *Adv. Funct. Mater.* **19**, 23, 3821-3832.

7 Ebner A.D., Gray M.L., Chisholm N.G., Black Q.T., Mumford D.D., Nicholson M.A., Ritter J.A. (2011) Suitability of a Solid Amine Sorbent for CO_2 Capture by Pressure Swing Adsorption, *Ind. Eng. Chem. Res.* **50**, 9, 5634-5641.

8 Li B., Jiang B., Fauth D.J., Gray M.L., Pennline H.W., Richards G.A. (2011) Innovative nano-layered solid sorbents for CO_2 capture, *Chem. Commun.* **47**, 6, 1719-1721.

9 Gray M.L., Hoffman J.S., Hreha D.C., Fauth D.J., Hedges S.W., Champagne K.J., Pennline H.W. (2009) Parametric Study of Solid Amine Sorbents for the Capture of Carbon Dioxide, *Energy Fuels* **23**, 4840-4844.

10 Jones C.W., Maginn E.J. (2010) Materials and Processes for Carbon Capture and Sequestration, *Chemsuschem.* **3**, 8, 863-864.

11 Hiyoshi N., Yogo K., Yashima T. (2005) Adsorption characteristics of carbon dioxide on organically functionalized SBA-15, *Micropor. Mesopor. Mater.* **84**, 1-3, 357-365.

12 Gray M.L., Champagne K.J., Fauth D., Baltrus J.P., Pennline H. (2008) Performance of immobilized tertiary amine solid sorbents for the capture of carbon dioxide, *Int. J. Greenhouse Gas Control* **2**, 1, 3-8.

13 Sircar S., Golden T.C. (1995) Isothermal and Isobaric Desorption of Carbon-Dioxide by Purge, *Ind. Eng. Chem. Res.* **34**, 8, 2881-2888.

14 Kim J.-N., Chue K.-T., Kim K.I., Cho S.-H., Kim J.-D. (1994) Non-isothermal Adsorption of Nitrogen-Carbon Dioxide Mixture in a Fixed Bed of Zeolite-X, *J. Chem. Eng. Japan* **27**, 45-51.

15 Merel J., Clausse M., Meunier F. (2008) Experimental investigation on CO_2 post-combustion capture by indirect thermal swing adsorption using 13X and 5A zeolites, *Ind. Eng. Chem. Res.* **47**, 1, 209-215.

16 Liu J., Wang Y., Benin A.I., Jakubczak P., Willis R.R., Levan M.D. (2010) CO_2/H_2O Adsorption Equilibrium and Rates on Metal-Organic Frameworks: HKUST-1 and Ni/DOBDC, *Langmuir* **26**, 17, 14301-14307.

17 Li G., Xiao P., Webley P., Zhang J., Singh R., Marshall M. (2008) Capture of CO_2 from high humidity flue gas by vacuum swing adsorption with zeolite 13X, *Adsorption* **14**, 2-3, 415-422.

18 Trzpit M., Soulard M., Patarin J., Desbiens N., Cailliez F., Boutin A., Demachy I., Fuchs A.H. (2007) The effect of local defects on water adsorption in silicalite-1 zeolite: A joint experimental and molecular simulation study, *Langmuir* **23**, 20, 10131-10139.

19 Dunne J.A., Mariwala R., Rao M., Sircar S., Gorte R.J., Myers A.L. (1996) Calorimetric heats of adsorption and adsorption isotherms .1. O_2, N_2, Ar, CO_2, CH_4, C_2H_6 and SF_6 on silicalite, *Langmuir* **12**, 24, 5888-5895.

20 Palomino M., Corma A., Rey F., Valencia S. (2010) New Insights on CO_2 – Methane Separation Using LTA Zeolites with Different Si/Al Ratios and a First Comparison with MOFs, *Langmuir* **26**, 3, 1910-1917.

21 Chatelain T., Patarin J., Soulard M., Guth J.L., Schultz P. (1995) Synthesis and characterization of high-silica EMT and FAU zeolites prepared in the presence of crown-ethers with either ethylene-glycol or 1,3,5-trioxane, *Zeolites* **15**, 90

22 Belmabkhout Y., Pirngruber G., Jolimaitre E., Methivier A. (2007) A complete experimental approach for synthesis gas separation studies using static gravimetric and column breakthrough experiments, *Adsorption* **13**, 3-4, 341-349.

23 Dunne J.A., Rao M., Sircar S., Gorte R.J., Myers A.L. (1996) Calorimetric heats of adsorption and adsorption isotherms. 2. O_2, N_2, Ar, CO_2, CH_4, C_2H_6, and SF_6 on NaX, H-ZSM-5, and Na-ZSM-5 zeolites, *Langmuir* **12**, 24, 5896-5904.

24 Li G., Xiao P., Webley P.A., Zhang J., Singh R. (2009) Competition of CO_2/H_2O in adsorption based CO_2 capture, *Energy Procedia* **1**, 1, 1123-1130.

25 Zhang J., Webley P.A. (2008) Cycle development and design for CO_2 capture from flue gas by vacuum swing adsorption, *Environ. Sci. Technol.* **42**, 2, 563-569.

26 Zhang J., Webley P.A., Xiao P. (2008) Effect of process parameters on power requirements of vacuum swing adsorption technology for CO_2 capture from flue gas, *Energy Convers. Manage.* **49**, 2, 346-356.

27 Liu Z., Grande C.A., Li P., Yu J.G., Rodrigues A.E. (2011) Multi-bed vacuum pressure swing adsorption for carbon dioxide capture from flue gas, *Sep. Purifi. Technol.* **81**, 3, 307-317.

28 Park J.H., Beum H.T., Kim J.N., Cho S.H. (2002) Numerical analysis on the power consumption of the PSA process for recovering CO_2 from flue gas, *Ind. Eng. Chem. Res.* **41**, 16, 4122-4131.

29 Chue K.T., Kim J.N., Yoo Y.J., Cho S.H., Yang R.T. (1995) Comparison of Activated Carbon and Zeolite 13X for CO_2 Recovery from Flue-Gas by Pressure Swing Adsorption, *Ind. Eng. Chem. Res.* **34**, 2, 591-598.

30 Na B.K., Lee H., Koo K.K., Song H.K. (2002) Effect of rinse and recycle methods on the pressure swing adsorption process to recover CO_2 from power plant flue gas using activated carbon, *Ind. Eng. Chem. Res.* **41**, 22, 5498-5503.

31 Dantas T.L.P., Luna F.M.T. Silva I.J., Torres A.E.B., de Azevedo D.C.S., Rodrigues A.E., Moreira R.F.P.M. (2011) Carbon dioxide-nitrogen separation through pressure swing adsorption, *Chem. Eng. J.* **172**, 2-3, 698-704.

32 Kikkinides E.S., Yang R.T., Cho S.H. (1993) Concentration and recovery of CO_2 from flue-gas by pressure swing adsorption, *Ind. Eng. Chem. Res.* **32**, 11, 2714-2720.

33 Pirngruber G.D., Hamon L., Bourrelly S., Llewellyn P.L., Lenoir E., Guillerm V., Serre C., Devic T. (2012) A Method for Screening the Potential of MOFs as CO_2 Adsorbents in Pressure Swing Adsorption Processes, *Chemsuschem.* **5**, 4, 762-776.

34 Liu Z., Wang L., Kong X., Li P., Yu J., Rodrigues A.E. (2012) Onsite CO_2 Capture from Flue Gas by an Adsorption Process in a Coal-Fired Power Plant, *Ind. Eng. Chem. Res.* **51**, 21, 7355-7363.

35 Cho S.-H., Park J.H., Beum H.T., Han S.-S., Kim J.-N. (2004) A 2-stage PSA Process for the Recovery of CO_2 from Flue Gas and its Power Consumption, *Stud. Surf. Sci. Catal.* **153**, 405-410.

36 Lively R.P., Chance R.R., Koros W.J. (2010) Enabling Low-Cost CO_2 Capture *via* Heat Integration, *Ind. Eng. Chem. Res.* **49**, 16, 7550-7562.

37 Lively R.P., Chance R.R., Kelley B.T., Deckman H.W., Drese J.H., Jones C.W., Koros W.J. (2009) Hollow Fiber Adsorbents for CO_2 Removal from Flue Gas, *Ind. Eng. Chem. Res.* **48**, 15, 7314-7324.

38 Sivakumar S.V., Rao D.P. (2011) Modified Duplex PSA. 1. Sharp Separation and Process Intensification for CO_2-N_2-13X Zeolite System, *Ind. Eng. Chem. Res.* **50**, 6, 3426-3436.

39 Kearns D.T., Webley P.A. (2006) Modelling and evaluation of dual-reflux pressure swing adsorption cycles: Part I. Mathematical models, *Chem. Eng. Sci.* **61**, 22, 7223-7233.

40 Diagne D., Goto M., Hirose T. (1994) New PSA Process with Intermediate Feed Inlet Position Operated with Dual Refluxes – Application to Carbon-Dioxide Removal and Enrichment, *J. Chem. Eng. Japan* **27**, 1, 85-89.

41 Diagne D., Goto M., Hirose T. (1995) Parametric Studies on CO₂ Separation and Recovery by a Dual Reflux PSA Process Consisting of Both Rectifying and Stripping Sections, *Ind. Eng. Chem. Res.* **34**, 9, 3083-3089.

42 Leinekugel-le-Cocq D., Tayakout-Fayolle M., Le Gorrec Y., Jallut C. (2007) A double linear driving force approximation for non-isothermal mass transfer modeling through bi-disperse adsorbents, *Chem. Eng. Sci.* **62**, 15, 4040-4053.

43 Farooq S., Ruthven D.M., Boniface H.A. (1989) Numerical simulation of a pressure swing adsorption oxygen unit, *Chem. Eng. Sci.* **44**, 12, 2809-2816.

APPENDIX

The cyclic PSA model is based on the non-isothermal adsorption column model described by Leinekugel-le-Cocq *et al.* [42]. It is summarized in Table A1 and Table A2. The main assumptions of the bed model are:

– the ideal gas law is obeyed;

– the pressure drop in the bed is negligible;

– the flow in the packed bed is represented by a cascade of CSTR (Continuous Stirred Tank Reactors) in series; 101 reactors have been used in the following simulations corresponding to a Péclet number of approximately 200;

– the adsorbent pellets have a bi-modal pore size distribution (micro- and macropores), and the intra-particle mass transfer is described by the modified double linear driving force model;

– chemical kinetic time constant is small compare to mass transfer time constant in the particle;

– adsorption equilibrium are modeled considering extended multi-component Langmuir isotherms.

During pressurization and blow-down steps, we consider that the total pressure in the bed changes linearly with time [43]:

$$P(t) = P_I^{step} + (P_F^{step} - P_I^{step}) \frac{t - t_I^{step}}{\Delta t_{step}} \tag{1}$$

The computing code based on this model has been developed in Fortran. The ordinary differential equations system obtained by spatial discretization by a cascade of CSTRs is solved using the DDASPK subroutine based on the Petzold-Gear BDF method.

TABLE A1

Cyclic PSA model

Models	Equations
CO_2 bulk phase mass balance	$\dfrac{\partial c_{CO_2}}{\partial t} = -\dfrac{1}{\varepsilon} \cdot \dfrac{\partial (u \cdot c_{CO_2})}{\partial z} - \dfrac{1-\varepsilon}{\varepsilon} \varepsilon_p \cdot a_s^p \cdot N_{CO_2}^{mac}$
Bulk phase energy balance	$\dfrac{\partial T_g}{\partial t} = -\dfrac{u}{\varepsilon} \cdot \dfrac{\partial T_g}{\partial z} + \dfrac{1}{C_{P,g}} \cdot \dfrac{\partial P}{\partial t} - \dfrac{1-\varepsilon}{\varepsilon} \cdot \dfrac{a_s^p \cdot k_{th}}{C_{P,g}} \cdot (T_g - T_s) - \dfrac{1}{C_{P,g}} \cdot \dfrac{2 \cdot k_w}{\varepsilon \cdot R_{int}} \cdot (T_g - T_w)$ with $C_{P,g} = \sum\limits_{i=1}^{n_c} c_i \cdot C_{P,i}$
Superficial u velocity expression: overall mass balance	$\dfrac{1}{\varepsilon} \dfrac{\partial u}{\partial z} = -\dfrac{1-\varepsilon}{\varepsilon} \cdot \dfrac{a_s^p \cdot k_{th}}{C_{P,g}} \cdot \left(1 - \dfrac{T_s}{T_g}\right) - \dfrac{1}{C_{P,g}} \cdot \dfrac{2 \cdot k_w}{\varepsilon \cdot R_{int}} \cdot \left(1 - \dfrac{T_w}{T_g}\right)$ $\qquad + \dfrac{\partial P}{\partial t} \cdot \left(\dfrac{1}{T_g} \dfrac{1}{C_{P,g}} - \dfrac{1}{P}\right) - \dfrac{1-\varepsilon}{\varepsilon} \cdot \varepsilon_p \cdot \left(\dfrac{R \cdot T_g}{P}\right) \cdot a_s^p \cdot N_T^{mac}$
CO_2 macroporous phase mass balance	$\dfrac{\partial c^{mac}}{\partial t} = a_s^p \cdot N_{CO_2}^{mac} - \dfrac{1-\varepsilon_p}{\varepsilon_p} \cdot a_s^c \cdot N_{CO_2}^{ads}$
N_T^{mac} expression: overall mass balance in macroporous phase	$N_T^{mac} = \dfrac{1}{a_s^p} \left(-\dfrac{P}{R \cdot T_s^2} \cdot \dfrac{\partial T_s}{\partial t} + \dfrac{1}{R \cdot T_s} \cdot \dfrac{\partial P}{\partial t} + \dfrac{1-\varepsilon_p}{\varepsilon_p} \cdot a_s^c \cdot N_{CO_2}^{ads}\right)$
CO_2 adsorbed phase mass balance	$\underbrace{\left(\dfrac{\partial q}{\partial c^*}\right)_{T_s} \cdot \dfrac{\partial c^*}{\partial t} + \left(\dfrac{\partial q}{\partial T_s}\right)_{c^*} \cdot \dfrac{\partial T_s}{\partial t}}_{\frac{\partial q}{\partial t}} = a_s^c \cdot N_{CO_2}^{ads}$
Particle energy balance	$\dfrac{\partial T_s}{\partial t} = \dfrac{a_s^c}{(1-\varepsilon_p) \cdot \rho_s \cdot C_s} \cdot N_{CO_2}^{ads} \cdot (-\Delta H_{CO_2}^{ads}) + \dfrac{a_s^p \cdot k_{th}}{(1-\varepsilon_p) \cdot \rho_s \cdot C_s} \cdot (T_g - T_s)$

TABLE A2

Intra-granular mass transfer molar flux and equilibrium

Models	Equations
CO$_2$ molar flow rate between bulk and macroporous phases	$$N_{CO_2}^{mac} = N_T^{mac} \cdot \frac{x_{CO_2}^{mac} \cdot e^{-N_T^{mac} \cdot \left(\frac{\delta_f}{D_{CO_2}^f \cdot c_T} + \frac{\delta_{mac}}{D_{CO_2}^{mac} \cdot c_T^{mac}} \right)} - x_{CO_2}}{e^{-N_T^{mac} \cdot \left(\frac{\delta_f}{D_{CO_2}^f \cdot c_T} + \frac{\delta_{mac}}{D_{CO_2}^{mac} \cdot c_T^{mac}} \right)} - 1}$$
CO$_2$ molar flow rate between macroporous and adsorbed phases	$$N_{CO_2}^{ads} = \frac{5}{R_c} \cdot D_{CO_2}^c \cdot \left(\frac{\partial q}{\partial c^*} \right)_{T_g} \cdot \left(c^{mac} - c^* \right)$$
Adsorption isotherm	$$\frac{q_{CO_2}}{q_{sat}} = \frac{b \cdot c^*}{1 + b \cdot c^*} \quad \text{with} \quad b = b_0 \cdot T_s \cdot e^{\frac{\Delta H_{CO_2}^{ads}}{R \cdot T_s}}$$